F. Fonte, S. Ricci, P. Mantegazza
Gust Load Alleviation for a Regional Aircraft Through a Static Output Feedback
Journal of Aircraft, Vol. 52, N. 5, 2015, p. 1559-1574
doi:10.2514/1.C032995

Gust Load Alleviation for a Regional Aircraft through Static Output Feedback

Fonte Federico[a] and Ricci Sergio[b] and Mantegazza Paolo[c]
Dipartimento di Scienze e Tecnologie Aerospaziali,

Politecnico di Milano, Milano, Italy, 27010

The paper presents the design of a symmetric active Gust Load Alleviation system for a regional transport aircraft, based on a Static Output Feedback with a constrained structure. The design is carried out on a comprehensive finite state aeroservoelastic model, including sensor units and actuator transfer functions, saturated in position, rate and hinge moment. The controller is designed within a quadratic optimal framework, through a second order, Hessian based, optimization algorithm, exploiting block diagonal Schur transformations of the closed loop state equations and performance weightings. An accurately chosen worst discrete gust and reference flight condition provide a baseline design, which is significantly effective in alleviating also continuous turbulence loads. Such a reference design proves itself robust enough to alleviate atmospheric loads over the complete flight envelope and is eventually further improved and robustified through a simple bilinear $q_\infty - M_\infty$ algebraic scheduling.

[a] Junior Researcher, Dipartimento di Scienze e Tecnologie Aerospaziali, Politecnico di Milano, Via La Masa 34.
[b] Associate Professor, Dipartimento di Scienze e Tecnologie Aerospaziali, Politecnico di Milano, Via La Masa 34.
[c] Professor, Dipartimento di Scienze e Tecnologie Aerospaziali, Politecnico di Milano, Via La Masa 34.

Nomenclature

$Diag[(\cdot)]$ = Diagonal matrix of the diagonal of a square matrix $(\cdot)$

h = Flight altitude [m]

$\mathbf{H}_{am}$, $\mathbf{H}_{a\Sigma^a m}$ = Aerodynamic transfer matrices due to structural motions

$\mathbf{H}_{ag}$, $\mathbf{H}_{a\Sigma^a g}$ = Aerodynamic transfer matrices due atmospheric motions

k = $\frac{\omega\, l_a}{V_\infty}$ Harmonic reduced frequency, imaginary part of p [$-$]

L = Turbulence scale [m]

l_a = Aerodynamic reference length [m]

M_∞ = Asymptotic Mach number, [$-$]

n_d = Denominator order of a rational transfer function

n_m = Numerator order of a rational transfer function

n_p = Number of design parameters

ω_0 = Natural frequency of a second order system [rad/s]

p = $\frac{s\, l_a}{V_\infty}$ Complex reduced frequency [$-$]

p_{wo} = Pole of a first order washout filter [rad/s]

$\mathbf{q}$ = Modal displacements vector

q_∞ = Asymptotic dynamic pressure, $[Pa]$

ρ_∞ = Asymptotic air density, [Kg/m^3]

s = Laplace variable [rad/s]

Σ^a = Aerodynamic contributions to internal loads

t_a = $\frac{l_a}{V_\infty}$, Aerodynamics reference time, $[s]$

V_∞ = Asymptotic air speed, $[m/s]$

v_g = Gust/turbulence velocity [m/s]

ξ = Damping factor [$-$]

I. Introduction

Atmospheric gusts and continuous turbulence can significantly affect aircraft ride qualities, increase airframe loads and be detrimental to on board equipments [24]. Their importance has

been recognized since the very beginning of aviation [20], and, by requiring the analysis of both discrete gusts and continuous turbulence, nowadays regulations impose stricter design requirements for atmospheric loads [1]. An optimized compliance with the related rules can be achieved through: an optimally strengthened airframe, active load reducing maneuvers, the integration of both. In such a view an early attempt toward active Gust Load Alleviation (GLA) was carried out in the late 1940s, on a Bristol Brabazon [34], which never went into production. In the late 1960s and early 1970s the USA further promoted the idea, supporting researches for an active gust load alleviation for the XB-70 bomber [29] and a more general Load Alleviation and Mode Suppression (LAMS) program [4]. Follow on applications of such researches could be devised in the operational applications to the Lockheed C-5A, Lockheed L-1001-500 and B-1 Lancer [40]. In the previously cited examples active GLA was added to already certified aircraft, so to extend their operational capabilities and be of help in solving unexpected marginal airframe problems. In fact, according to [10], prior to the 1980s that was a general tendency in the use of automatic control in aeronautical applications. Later on, instead, since its all wing design made it very sensible to gust/turbulence loadings, the GLA system of the B-2 bomber was designed from scratch along with its inception [12], [40]. In Europe, from 1976 to 1982 Dornier GMBH and DFVLR developed and tested a system named Open Loop Gust Load Alleviation (OLGA) [40]. It was based on a measurement of the angle of attack and was designed to operate within a low frequency range: i.e. between 0.3 and 1.0 Hz. It eventually became part of a Load Alleviation and Ride Smoothing (LARS) system, developed by the DLR [23], [40], whereas the open loop controller was used for the low frequency alleviation, while the overall aeroelastic response of the aircraft was regulated by a feedback controller. In recent years the development of lighter and more efficient transport aircraft has led to a widespread increase of the emphasis put on atmospheric load reduction, leading to commercial aeroplanes, e.g. the Airbus A380 and the Boeing 787, natively equipped with active controllers for load alleviation and comfort enhancement [40]. Moreover, new classes of vehicles, such as High Altitude Long Endurance (HALE) aircraft [49] and sensorcraft [31], because of their stronger weight reduction specifications, make it mandatory the use of active GLA systems as well. Finally, an aggressive combination of Manoeuvre and Gust Load Alleviation (MLA&GLA) technologies could be necessary in the case of more advanced aerodynamic

designs, such as those based on the Natural Laminar Flow (NLF) concept, holding the potential of significantly improving both the weight and the aerodynamic terms of the well known Breguet range equation.

The active GLA system developed in the present work is based on a Static Output Feedback (SOF) controller. The design of the related gain matrix is carried out within the framework of a quadratic optimal control, whose cost function is optimized by using a second order, Hessian based, algorithm, having as unknowns just the elements of an algebraic gain matrix and, even if not used in the present work, any system parameter available as design element.

The great simplicity of SOF controllers makes them advisable in many applications where simple control laws are desired. For example they are particularly well suited for massively controlled distributed systems, whereas actuator clusters are commanded only through a co-located set of sensors [32]. To increase its overall performance, it would be easy to complement a SOF with a low order dynamic regulator, designing the coupled static-dynamic controller through the same tools used for a purely static counterpart [44]. Owing to their simplicity, SOF regulators can also be used as backups, activated after a failure of a master system [5]. Another situation in which SOF design techniques can be used occurs when some parameters of an existing controller must be (re)tuned, while preserving its structure [30]. Finally, it is far simpler to schedule and interpolate the elements of a SOF gain matrix than the parameters of a dynamic controller, making it suitable for varying operating conditions.

An example of an aeronautical application of SOF controllers is provided by the work of Patil and Hodges [38], where a SOF was used for the flutter suppression and gust alleviation of a HALE. They also showed that a proper choice of the sensor locations provided results similar to those achievable by the use of an ideal full state Linear Quadratic Regulator (LQR). Miyazawa and Dowell [35] used a SOF flutter suppression based on a multi models approach, i.e. weighting several different models within a single quadratic cost function, thus leading to a controller insensitive to the uncertainties structured within the accounted models. A further SOF active flutter suppression, using a direct digital design and including a size constrained dynamic compensator, can be found in [13].

A common optimization approach of a SOF is based on the solution of Lyapunov equations, hav-

ing the closed loop state matrix as coefficients. Within such a framework, many existing algorithms support a first order, gradient based, optimization, such as the, legacy, Levine–Athans algorithm [28], often revised as in [36], while a different approach can be found in Anderson–Moore [3]. Second order optimization algorithms have also been proposed, [8], [16] and [17], where the optimization is carried out on a state variance matrix instead than on the gain matrix, with the result of being computationally very expensive when dealing with relatively large problems. Anderson–Moore method [3] was modified to achieve super linear convergence in [45], by introducing an approximation of the gain Hessian matrix. In [39] it was further enhanced with the computation of exact second derivatives of the cost function with respect to the gain matrix. Actually, its implementation was based on the iterated solution of a system of three coupled matrix equations, without any explicit actual calculation of the gain Hessian matrix. Another, often used, solution method is the adoption of general purpose, state of the art, optimization functions, either unconstrained or constrained, for which the user has to provide the support to compute its own objective, gradient and, possibly, Hessian [26] and [37].

This work will develop and adopt its own Lyapunov based method, providing a simple and direct second order approximation of the objective function by effectively calculating its true gain Hessian matrix, so that the optimization can be carried out specifically as an iterated solution of the stationary condition, through a simple Levenberg-Marquardt modified Newton-Raphson iteration.

A more recent alternative approach to SOF design is based on its formulation as a system of Linear Matrix Inequalities (LMI) [11]. LMI based designs can take into account a varied set of requirements and constraints, but their computational demand can be high [30], especially for relatively large order systems. A few comparisons of the results provided by LMI and Lyapunov based approaches are presented in [21] and [30].

This paper summarizes the design, the implementation issues and the results obtained by applying a static output feedback controller to the gust/turbulence alleviation of a two engines regional transport aircraft. It is organized as follows: section II introduces the aeroelastic model and the gust/turbulence input considered for this research; section III describes the adopted control design guidelines, including their objectives and layout; section IV describes the controller optimization;

section V reports the actual control design as well as its verification results, while section VI draws some conclusions.

II. Aeroelastic model and gust/turbulence input

The main goal of this work is the design of the active gust alleviation system for a next generation regional transport aircraft, whose main geometrical and mass data are summarized in Tab. (1). ~~This model is freely inspired to the the Green Regional Aircraft (GRA), under development within the Clean Sky research program with the aim to develop and test new technologies to reduce the enviroinmental impact of aircraft.~~

overall length	40.69 m	wing span	34.96 m	horizontal tail span	12.30 m
overall height	7.884 m	wing root chord	5.453 m	horizontal tail root chord	3.762 m
Total mass	52266 Kg	wing tip chord	1.498 m	horizontal tail tip chord	1.349 m

Table 1 ~~*GRA*~~ *geometric properties.*

~~Its~~ aeroelastic model has been obtained through the use of NeoCASS [14], [15], a GPLled open source suite of Matlab modules combining state of the art computational, analytical and semi-empirical methods, tackling all the aspects of a conceptual aero-structural analysis (www.neocass.org). Starting from a reduced set of aircraft geometrical data and mission requirements a fairly detailed conceptual sizing of the airframe and its mass distribution has been easily determined by using NeoCASS Weights-Balance (WB) and Generic Unknowns Estimator and Structural Sizing (GUESS) modules.

A. Structural and aerodynamic models

The NeoCASS symmetric structural stick model, generated through its own aeroelastic design, is shown in Fig. 1a. It is composed of 53 beams: 10 for the fuselage, 18 for the wing, 11 for the vertical tail and 14 for the horizontal tail.

NeoCASS symmetric dynamic analyses have been successively validated through the use of NASTRAN [42]. The first wing bending mode of the aircraft has a frequency of 3.76 Hz, while its clean laminar wing has a very high torsional stiffness, driving the first wing torsional mode up to

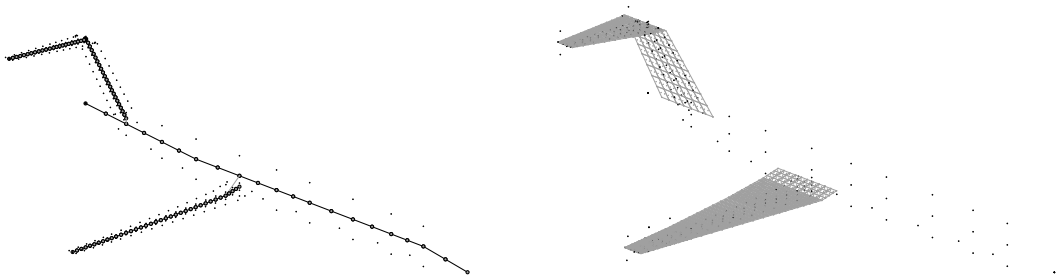

(a) *Structural model.* **(b)** *Aerodynamic model.*

Fig. 1 *Structural and aerodynamic models.*

31.74 Hz. An overview of a few significant low frequency vibration modes is presented in Tab. (2). Both NeoCASS and NASTRAN showed no flutter for all configurations within the design flight envelope, its only mild, long term, numerical instability being related to the integrator associated to the simply stable plunge mode at the imposed straight and level flight speed.

frequency $[Hz]$	Description
3.763	First wing bending
4.784	Wing and fuselage bending
9.339	Horizontal tail and fuselage bending
9.662	First wing in-plane bending
12.205	Second wing bending

Table 2 *Selected low frequency vibration modes.*

The Doublet Lattice (DL) [2] based aerodynamic mesh shown in Fig. 1b is composed by 1000 panels, 764 on the wing and 180 on the horizontal tail. It provides the converged harmonic Generalized Aerodynamic Forces (GAF) associated to the lowest 19 vibration modes of the free-free aircraft and gust boundary conditions. Such a relatively high number of modes is strictly not required for well converged motion responses, but, combined with a mode acceleration based on the direct summation of the unsteady aerodynamic loads, ensures the obtainment of well converged internal forces.

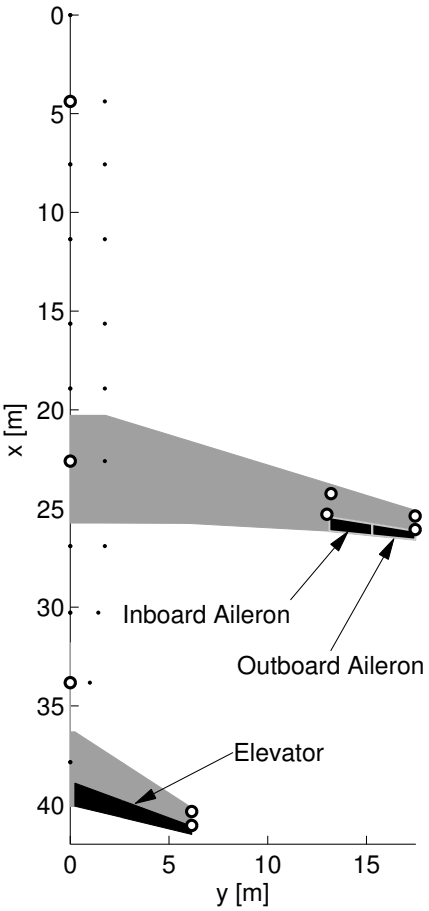

Fig. 2 *Aircraft control surfaces and accelerometer locations* (○).

B. Control surfaces and actuators

The aircraft has five control surfaces: a doubly split aileron, elevator, and two flaps. Since any conceivable bandwidth of the actuators controlling the flaps will not be adequate to provide any gust load alleviation, only the elevator and the ailerons will be exploited for the design of the control system, as shown in Fig. (2).

The two ailerons can be moved either independently or with the same command. It is anticipated that the best control will be chosen by comparing the design performances obtainable for each of the two operational modes.

The control surfaces are left free to move within the vibration mode calculations, their dynamics is thus mostly determined by the position servo-actuators controlling them. The related compliant

servos are approximated through a transfer function of the form:

$$\delta(s) = \frac{\omega_0^2}{s^2 + 2\xi\omega_0 s + \omega_0^2}\delta_c(s) - \frac{M_h(s)}{K_\delta} \qquad |\delta| \leq \delta_s \qquad |\dot{\delta}| \leq \dot{\delta}_s \qquad |M_h| \leq M_{hs} \qquad (1)$$

where δ is the control surface deflection, δ_c the commanded deflection, M_h the hinge moment and K_δ the residualized static approximation of the lumped stiffness transfer function related to the actuator and its mounting structure, the s suffix indicating the related saturation values. The values of ξ and ω_0 are chosen so to provide a flat nominal $3dB$ passband of 3.25 Hz for the aileron and 0.95 Hz for the elevator. For both control surfaces K_δ is preliminarily given a value leading to a reasonably assumed, control surface only, oscillating frequency of about 30 Hz.

Clearly, the nonlinear saturations, δ_s, $\dot{\delta}_s$ and M_s, cannot be cared of in a linear controller design, but will be accounted for in the time domain simulations aimed at its validation.

It might be likely that, while the bandwidth of the elevator transfer function is well within the reach of the actual technology, that of the aileron is a somewhat demanding requirement. Nevertheless it is the lowest specification allowed for a sizeable reduction of the wing bending moment, as obtained through repeated designs of the type presented in the following parts of the paper.

C. Finite State Space Approximation of the Aerodynamics

To provide a state space model for the whole aeroservoelastic system a finite state Linear Time Invariant (LTI) approximation of the aerodynamic model has to be adopted. Therefore, a matrix fraction representation of the aerodynamic transfer matrices [41] has been determined:

$$\mathbf{H}_a(p, M) = \mathbf{D}^{-1}(p, M)\mathbf{N}(p, M) \qquad (2)$$

where $\mathbf{H}_a(p, M)$ is the aerodynamic transfer matrix, with $\mathbf{D}(p, M)$ and $\mathbf{N}(p, M)$ being matrix polynomials in the reduced Laplace variable $p = sl_a/V_\infty = \sigma l_a/V_\infty + j\omega l_a/V_\infty = h + jk$. The aerodynamic contributions to the internal loads are computed at selected points of the airplane structure, e.g. the wing root, and are recovered through the mentioned mode acceleration method. Thus, the aerodynamic transfer matrix is augmented to include the contribution of the aerodynamic

forces to the internal load at such points, resulting in

$$\begin{Bmatrix} \mathbf{Q_a} \\ \mathbf{\Sigma_a} \end{Bmatrix} = \begin{bmatrix} \mathbf{H_{am}} & \mathbf{H_{ag}} \\ \mathbf{H_{a\Sigma^a m}} & \mathbf{H_{a\Sigma^a g}} \end{bmatrix} \begin{Bmatrix} \mathbf{q} \\ \frac{v_g}{V_\infty} \end{Bmatrix} \tag{3}$$

where $\mathbf{Q_a}$ is the vector of the GAFs, $\mathbf{\Sigma_a}$ the contribution of the aerodynamic forces to the internal stresses of interest, $\mathbf{q}$ the vector of the modal amplitudes, and $\frac{v_g}{V_\infty}$ the gust/turbulence input. The numerator matrix polynomial $\mathbf{N}(p, m)$ is an order of two higher than that of $\mathbf{D}(p.M)$ and thus the resulting transfer function is not strictly proper and can be expressed as:

$$\mathbf{H}(p, M) = \mathbf{D_0} + p\mathbf{D_1} + p^2\mathbf{D_2} + \mathbf{C}(p\mathbf{I} - \mathbf{A})^{-1}\left(\mathbf{B_0} + p\mathbf{B_1} + p^2\mathbf{B_2}\right) \tag{4}$$

The presence of the terms $\mathbf{D_1}$, $\mathbf{D_2}$, $\mathbf{B_1}$ and $\mathbf{B_2}$ comes from the mentioned non strictly proper assumption, indicating that system input is not only the input vector $\begin{bmatrix} \mathbf{q} & \frac{v_g}{V_\infty} \end{bmatrix}^T$, but also its first and second time derivatives. The inclusion of these derivatives can be interpreted as a low frequency residualization of the high frequency part of the aerodynamics. See also the following comments in relation to keeping such a second order residualization for the generalized gust forces.

D. Gust and turbulence

The time shape and amplitude of discrete gusts is prescribed by airworthiness regulations. The European Aviation Safety Agency (EASA) [1] dictates a *1-cos* shape for deterministic gusts

$$v_g = \begin{cases} \frac{U_g}{2}\left[1 - \cos\left(\frac{\pi s}{H}\right)\right] & 0 < s \leq 2H \\ 0 & s > 2H \end{cases} \tag{5}$$

where s is the gust penetration distance, H the gust gradient and U_g the peak gust velocity in equivalent airspeed, which depends upon the gust length and altitude. The gust profiles for various values of H are shown in Fig. 3a, where their amplitudes have been computed by assuming a flight altitude of 8000 m and an air density $\rho_\infty = 0.53\ kg/m^3$.

It is remarked that a *1-cos* gust has a simple jump discontinuity in its second time derivative, so it poses no problem to a second order residualization of its generalized aerodynamic forces. Since, as it will be seen in a following section, the adopted optimal quadratic formulation will be based only on a response optimization with respect to impulsive and white noise disturbances, a

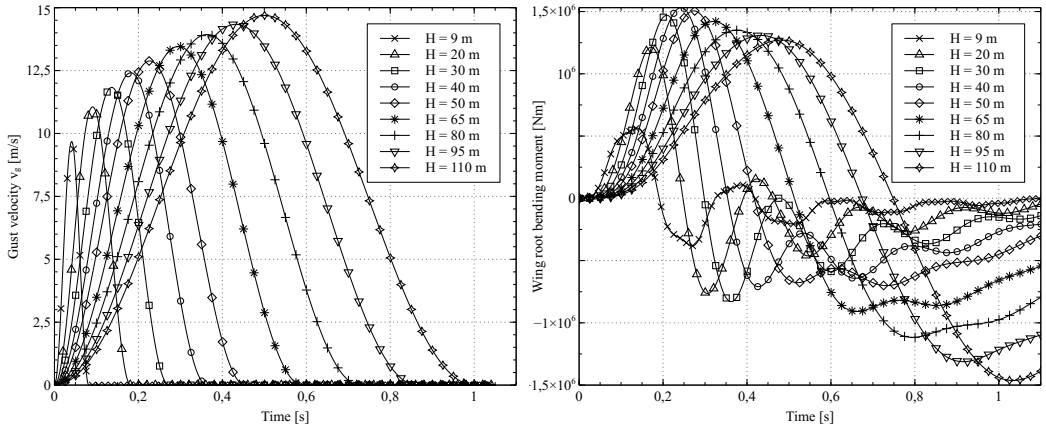

(a) *Gust profiles.* **(b)** *Related wing root bending moments.*

Fig. 3 *Overview of different gust gradients H, at: $M = 0.71$, $q_\infty = 1.282 \times 10^4$ Pa, $h = 8000$ m.*

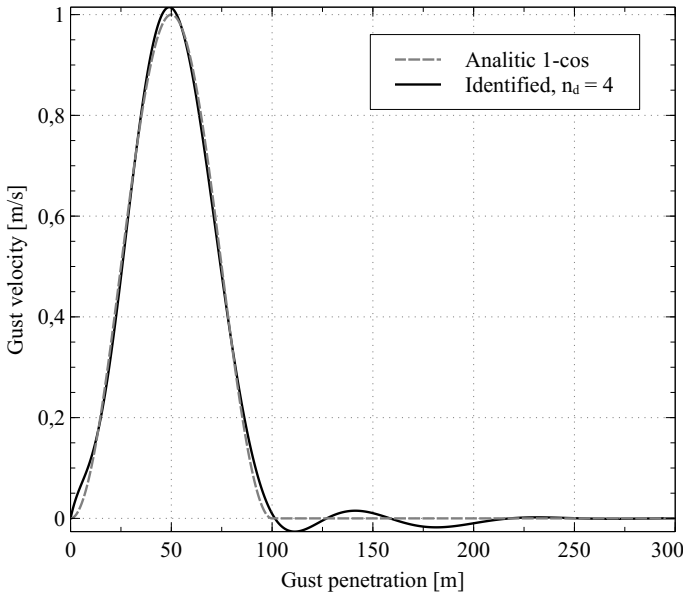

Fig. 4 1-cos *gust and shaping filter for $H = 50$ m..*

deterministic LTI shaping filter is needed to well match a *1-cos* gust shape through the application of appropriate impulses. So the *1-cos* shape is approximated as an impulse response by matching its Fourier transform through a non linear least squares identification [41]. A sample result of such an identification, based on a strictly proper rational filter with four poles and two zeroes, for $H = 50$ m, is shown in Fig. 4.

According to EASA regulations, also continuous turbulence loads, with a Von Karman Power

Spectral Density (PSD), must be taken into account. Such a model well approximates experimental data, but, due its non rational form, it is precisely matched only by a relatively large order time invariant shaping filter. Thus the simpler Dryden spectrum [48]:

$$\Phi(\Omega) = \frac{\sigma_w^2 L}{\pi V_\infty} \frac{1 + 3\left(\frac{\omega L}{V_\infty}\right)^2}{\left[1 + \left(\frac{\omega L}{V_\infty}\right)^2\right]^2} \tag{6}$$

is retained to be an adequate approximation for our design aims. It should be noticed that it has a $1/\omega^2$ asymptotic frequency decay. Therefore, to avoid the time derivative of the white noise, a fictitious high frequency pole is added to its own shaping filter, ending with:

$$H_{gsf}(s) = \sigma_w \sqrt{\frac{L}{\pi V_\infty}} \frac{1 + \sqrt{3}\frac{sL}{V_\infty}}{\left(1 + \frac{sL}{V_\infty}\right)^2 \left(1 + \frac{sL}{100\, V_\infty}\right)} \tag{7}$$

It is here anticipated that, following a set of extended simulations, a deterministic gust will drive the design of our load alleviation system. Such a choice is related to the extended frequency content of the chosen gust profile, capable of exciting an adequate frequency range, wider than that of the continuous turbulence, over the all flight envelope. Therefore, a good discrete gust design will invariably lead to an at least as good turbulence alleviation.

III. Control Design Guidelines: objectives and layout

The term Static Output Feedback is often a kind of misnomer as, even if it is true that it is related to a design directly feeding back a set of given output, it is not said that they are related only to actual measures. In fact, as it will be shown shortly, a significant part of the design of a SOF might be devoted to setting up an appropriate processing of the available measurements so to enrich the controller with structurally constrained and easy to realize compensations, further improving its effectiveness. It is then of interest to highlight the feature of such a design part for the problem at hand.

Furthermore, the simplification associated to a SOF controller should not significantly penalize its performances with respect to a supposedly better more complex solutions. In such a view an LQG-LTR reference design will be carried out in parallel, determining its state feedback and observer by using the same augmented aeroservoelastic model part previously presented, along with all the filters and compensations to be shortly presented. The adoption of such a reference solution is based

on past experiences, which have shown that with the frequency weighting implied in the adopted design model, an LQG-LTR solution can be quite robust and effective. Eventually, to simulate a truly viable implementation, a reduced order LQG-LTR controller will be the one used for the actual comparisons, always caring to keep it close to its full order best performances. Since the SOF controller will anyhow provide a far simpler structure than its reduced order LQG-LTR counterpart, a fair check of the (dis)advantages of each solution should be of help in evaluating the possible merits of the preference given to a SOF solution.

A. Control objectives

The main objective of the alleviation system is to reduce the internal loads acting on the airframe under gust/turbulence loads. Since one of the related most critical points for the airframe is the wing root, its shear, bending and torsional moment will be taken as the main control objectives, the root bending moment being the reference performance for comparing various controller designs. Nevertheless, the achievement of the above objective should not penalize other significant internal loads unduly. Therefore, further guard objectives will be set on the internal forces at the horizontal tail plane root and at the fuselage section just behind the wing root. In addition to a load alleviation, the control system should also provide some ride quality enhancement, thus enforcing the need of keeping under control a few accelerations along the fuselage. Finally, all of what above cannot be separated from the whole aircraft longitudinal flight mechanics, with the consequent need of keeping the state of aircraft motion as a part of the performances to be controlled. Nevertheless, the SOF controller activity on the aircraft state should emphasize its load alleviation function, coupled to a mild stabilization of the mentioned long term instability related to the model approximation, already pointed out in the aeroelastic modeling paragraph. Therefore, it should have a low authority interaction with the maneuvers commanded by a possible external flight control system.

According to the airworthiness rules the above objectives should be achieved both for discrete gusts and continuous turbulence, so setting the need of a multi objective optimization, somewhat mimicking a mixed H_2/H_∞ design. Nonetheless, a comprehensive initial design familiarization phase has shown that the choice of an appropriate discrete gust condition could have confidently been adopted as a reference design point, adequate enough to provide acceptable performances also

for a continuous turbulence, thus simplifying the design process significantly. As already anticipated, such a choice finds its justification in the wider frequency content of the discrete design gust with respect to the turbulence design spectrum, which shows less demanding control actions.

In such a view, an adequate baseline design has been set at a reference flight condition characterized by $M_\infty = 0.71$ and $V_\infty = 220\ m/s$, for a worst discrete gust having a gradient of $H = 40\ m$.

In order to assess the robustness of the controlled system, the gain and phase margins for the simultaneous breaking of all input loops were evaluated [9] and the design weights tuned to guarantee the right compromise between the previously illustrated design objectives and a close attainment of a $\pm 6\ dB$ gain and $\pm 45^\circ$ phase margins.

No bandwidth specification is assigned, as it is implicitly defined by having fully taken into account in the design model the dynamics of the actuators, already presented, and the sensors, to be described next.

It should be now remarked that, apart from the precise statement of the control margins and implied bandwidth, the somewhat loose specifications set above are what is needed to define a quadratic performance index, which will drive the actual determination of the controller parameters, whose structure, i.e. feedback paths layout, measurements and their compensations, are an assigned designer's choice.

Then, the satisfaction of the varied specification set will be the outcome of appropriately iterated verifications over the weights defining the quadratic objective function.

B. Controller layout

As previously stated the controller can either move the whole aileron with a single control law or provide separate commands to each split part. Even if the former needs only a single actuator resulting in a simpler and more economical system, it is likely that a coordinated double actuation is better suited to help in satisfying the bandwidth requirements. In fact many in service commercial aircraft, already have a doubly split ailerons for their flight control and load alleviation purposes. Thus, both the design of a single coordinated and a double independent actuation, will be carried out, the more complex split solution being preferred only if it will achieve better performances.

Since the layout of the measurements and their compensation is an important part of the de-

sign of a direct feedback controller, the next paragraph is specifically deserved to them. Moreover, it is here anticipated that we will also explore both a full direct feedback of each measure and compensatied output to the actuators and a partially decoupled design. In fact, in view of further simplifying the structure of the controller, the latter will constrain the feedback paths in a loosely co-located way, i.e. all the measurements and compensations taken at the tail will affect only the elevator motion, while those taken at the wing will command the ailerons. All the other measurements, fuselage sensors, specifically installed for the load alleviation, and the available Inertial Measurement Unit (IMU) flight mechanics data, being fed back to both.

C. Measurements and Compensations

The choice of the type of sensors, along with their positioning and compensation to derive further signals enriching the knowledge of the structural motions, are an essential part of the designer guided design associated to a SOF. In our case, albeit being far away from the ideal one, it is driven by the idea of a close co-location of the sensed motions and the aerodynamic control forces. Moreover, as already said, they should serve a substantially stand alone internal control loop, at a relatively high frequency, not unduly interfering with the flight control system.

Along the above cited guidelines the basic sensors employed will be a set of accelerometers, in the direction normal to the lifting surfaces, placed at selected points on the wing, fuselage and horizontal tail plane. Their transfer function is designed so to be unified by the following model:

$$a_{meas} = \frac{s}{(s + p_{wo})} \cdot \frac{\omega_o^2}{(s^2 + 2\xi\omega_0 s + \omega_0^2)} a \tag{8}$$

which will become part of the system state, with a_{meas} becoming the related strictly proper output of the actual acceleration a. Its first order part is clearly a standard wash out filter, aimed at reducing the interference with the flight control system. The second order part is to be associated mainly to the anti aliasing filter required by a digital implementation. In fact any viable accelerometer choice will feature a significantly wider low pass band than the one to be sampled, thus there is only need to care for a gain and phase adequate to well measure the frequency range of the modes of interest, i.e. between 3 and 30 Hz. It should be remarked that the wash out filter is embedded in the accelerometer itself in the case of the choice of a piezoelectric type. In accordance with what

said above the high pass band will be set at 0.3 Hz and the second order low pass at 35 Hz, in a 3 dB attenuation sense.

From the accelerometers it is possible to derive the co-located elastic velocities, v, and displacements, d, through an approximated double integration, of the type:

$$v = \frac{s}{s^2 + 2\xi\omega_0 s + \omega_0^2} a_{meas} \qquad\qquad d = \frac{s}{s^2 + 2\xi\omega_0 s + \omega_0^2} v \tag{9}$$

with $f_0 = \frac{\omega_0}{2\pi} = 0.2\ Hz$, which, by rejecting biases and low frequency drifts, allows safe long term integrations, providing an approximation close to the ideal $1/s$ within the range of the previously given modes of interest. The above integrations must not be interpreted as an open loop compensation. In fact they will become a part of the final design model, so that their output will be a combination of the system state components.

From the implementation point of view it should be noticed that both the accelerometer filters and the integrators can be realized analogically, each unit providing three output to be sampled. Alternatively one could sample just the accelerometer output and code the wash out filter, if it is not of the piezoelectric type, along with the double integrators, within the control computer. Whatever solution is chosen, all together, they will provide an integrated three output sensing unit. As a further notice it is pointed out that, contrarily to the actuators, possible sensor saturations will be guarded, but not cared of, during the design verifications. In fact, it is worth anticipating that none ever happened.

Six such sensing units will be placed across a few span wise locations of the aerodynamic surfaces: two at the wing tip, two at about 75% of the wing span, two at the tip of the horizontal tail, so that each couple can sense the related section bending and torsional motions.

Another three sensing units will be located along the fuselage, one at the nose, one at the wing root crossing, one at the tail. The position of all of them is sketched in Fig. (2).

In addition to sensing peculiar elastic motions a set of complementary measures are assumed to be available for free, i.e. the control surface deflections and the state of the aircraft reference frame. The former should come from the actuators servo positioning, while the latter, in terms of: altitude, pitch and their rates, from an Inertia Measurement Unit (IMU) of adequate quality, whose installation on an aircraft of the kind to be designed is taken for granted. Their dynamics and anti

aliasing filters are modeled as first order low pass at 10 Hz.

D. Delay Filter

A SOF of the kind here adopted requires a digital implementation. Taking into account the digitalization of the wash out filter and the double integration associated to the accelerometer based sensing units, the per sample number of multiply-add operations will, roughly, be in the range of 150. Therefore, even for a nowadays low end control computer and data acquisition, the related delay is estimated to be sub millisecond, thus well tolerated within the previously specified phase margins. Consequently, the digital delay will mostly be related to the output sample and hold, i.e. half of the sampling time, which, assuming a conservative 100 Hz sampling frequency, amounts to 5 milliseconds. Such a not so negligible delay will erase a significant part of the phase margin, so it must be cared of when designing a continuous SOF gain matrix. Therefore, a standard Padé transfer function is placed in series to each of the three control output, adopting a strictly proper rational approximation [46], with a numerator of order 4 and denominator of order 5. The strictly proper rational Padé approximation is preferred to its simply proper counterpart of the same order, because it provides a no jump initial transient, as shown in Fig. (5), where the two are compared. It should be noticed also that, to avoid hybrid simulations, the above continuous approximation of

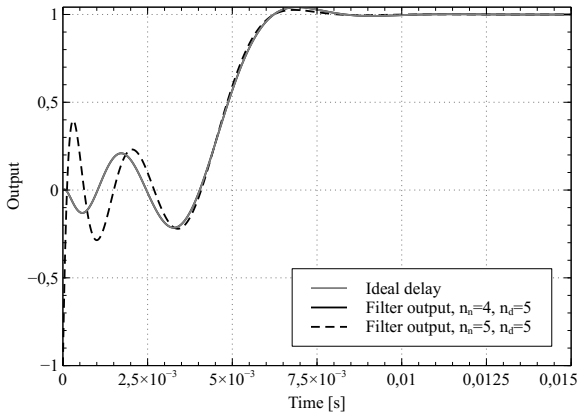

Fig. 5 *Padé filter step responses, delay $\tau = 5\ ms$.*

the digital delays will be kept, as it is, also for the post design verifications.

E. Complete Model

The final aircraft model adopted for designing the SOF controller comprises the following number of states:

- 38: structure; 19 structural modes: 6 rigid, airframe motion and control rotations, 13 deformable.
- 20: aerodynamics.
- 6: actuator transfer functions.
- 63: 9 accelerometer based sensing units; 7 states each: wash out plus 2 integrators.
- 15: 3 delay filters.
- 4: low pass, IMU.
- 3: low pass, control surface deflections.
- 4: discrete gust shaping.

totalling 153 states and 34 measurement output.

IV. Controller Optimization

This section presents the second order optimal quadratic formulation adopted to finalize the design of a SOF controller. Even if it will not be exploited in this work, the chosen approach can combine the related feedback design with the optimization of any other system parameter, thus making it possible the integrated tuning of different design facets, e.g. passive and active components, placement of sensors and actuators and their technological requirements.

A. Quadratically Optimized SOF Controller

Considering the generic Linear Time-Invariant (LTI) model

$$\begin{cases} \dot{\mathbf{x}} = \mathbf{A}\mathbf{x} + \mathbf{B}_u\mathbf{u} + \mathbf{B}_d\mathbf{d}, \\ \mathbf{y} = \mathbf{C}_y\mathbf{x} + \mathbf{D}_{yu}\mathbf{u} + \mathbf{D}_{yd}\mathbf{d} + \mathbf{n}, \\ \mathbf{z} = \mathbf{C}_z\mathbf{x} + \mathbf{D}_{zu}\mathbf{u} + \mathbf{D}_{zd}\mathbf{d}. \end{cases} \tag{10}$$

where $\mathbf{x} \in \mathbb{R}^n$ is the state vector, $\mathbf{u} \in \mathbb{R}^{m_u}$ the available control input, $\mathbf{d} \in \mathbb{R}^{m_d}$ the external disturbances, $\mathbf{y} \in \mathbb{R}^{l_y}$ the measures, corrupted by the noise $\mathbf{n} \in \mathbb{R}^{m_n}$, $\mathbf{z} \in \mathbb{R}^{l_z}$ the response performances of interest. A SOF controller will provide the control input $\mathbf{u} = -\hat{\mathbf{G}}\mathbf{y}$, which, by exploiting the definition of $\mathbf{y}$ in Eq. (10), can be rewritten as:

$$\mathbf{u} = -\left(\mathbf{I} + \hat{\mathbf{G}}\mathbf{D}_{yu}\right)^{-1}\hat{\mathbf{G}}\left(\mathbf{C}_y\mathbf{x} + \begin{bmatrix}\mathbf{D}_{yd} & \mathbf{I}\end{bmatrix}\begin{Bmatrix}\mathbf{d}\\ \mathbf{n}\end{Bmatrix}\right) = -\mathbf{G}\left(\mathbf{C}_y\mathbf{x} + \hat{\mathbf{D}}_y\hat{\mathbf{d}}\right) \tag{11}$$

with $\mathbf{G}(\hat{\mathbf{G}}) = \left(\mathbf{I} + \hat{\mathbf{G}}\mathbf{D}_{yu}\right)^{-1}\hat{\mathbf{G}}$, leading to the following closed loop system dynamics and performances:

$$\begin{cases} \dot{\mathbf{x}} = (\mathbf{A} - \mathbf{B}_u\mathbf{G}(\hat{\mathbf{G}})\mathbf{C}_y)\mathbf{x} + \begin{bmatrix}(\mathbf{B}_d - \mathbf{B}_u\mathbf{G}(\hat{\mathbf{G}})\mathbf{D}_{yd}) & -\mathbf{B}_u\mathbf{G}(\hat{\mathbf{G}})\end{bmatrix}\begin{Bmatrix}\mathbf{d}\\ \mathbf{n}\end{Bmatrix} = \hat{\mathbf{A}}\mathbf{x} + \hat{\mathbf{B}}\hat{\mathbf{d}} \\ \mathbf{z} = (\mathbf{C}_z - \mathbf{D}_{zu}\mathbf{G}\mathbf{C}_y)\mathbf{x} \quad + \begin{bmatrix}(\mathbf{D}_{zd} - \mathbf{D}_{zu}\mathbf{G}(\hat{\mathbf{G}})\mathbf{D}_{yd}) & -\mathbf{D}_{zu}\mathbf{G}(\hat{\mathbf{G}})\end{bmatrix}\begin{Bmatrix}\mathbf{d}\\ \mathbf{n}\end{Bmatrix} = \hat{\mathbf{C}}_z\mathbf{x} + \hat{\mathbf{D}}_z\hat{\mathbf{d}}. \end{cases} \tag{12}$$

The gain matrix $\mathbf{G}(\hat{\mathbf{G}})$ is computed by minimizing a user defined quadratic performance index J of the type:

$$J = E\left(\mathbf{z}^T\mathbf{W}_{zz}\mathbf{z} + \mathbf{u}^T\mathbf{W}_{\mathbf{uu}}\mathbf{u}\right). \tag{13}$$

with the definition of the expected value E depending upon the characterization chosen for the vector $\hat{\mathbf{d}}$, here modelled either as an impulse or as a null mean white noise. In the former case, the related expectation will be the covariance over the set of all possible impulse intensities while in the latter case, assuming ergodicity, it will be the time averaged correlation over any representative casual realization. Such expectations allow to define the disturbance covariance matrix:

$$E\left(\hat{\mathbf{d}}\,\hat{\mathbf{d}}^T\right) = \begin{bmatrix}\mathbf{V}_{dd} & \mathbf{V}_{dn}\\ \mathbf{V}_{nd} & \mathbf{V}_{nn}\end{bmatrix}. \tag{14}$$

It must now be remarked that having the term $\hat{\mathbf{D}}\,\hat{\mathbf{d}}$ in a quadratic performance implies an inappropriate multiplication of impulses and white noises. So if any such term does appear in $\mathbf{z}$ it will be either assumed to be negligible or forced to be part of the state $\mathbf{x}$ through an appropriate shaping filter, the convenience of filtering the components of $\mathbf{z}$ containing $\hat{\mathbf{d}}$ or $\hat{\mathbf{d}}$ itself being a designer's choice. It goes without saying that whenever such a choice will be applied directly to any component

of $\hat{\mathbf{d}}$, it will make it a state component, so disappearing from the corresponding disturbance term of all the closed loop system equations. It will be therefore always possible to write:

$$J = E\left(\mathbf{z}^T\mathbf{W}_{zz}\mathbf{z} + \mathbf{u}^T\mathbf{W}_{\mathbf{uu}}\mathbf{u}\right) = Tr\left[\left(\hat{\mathbf{C}}_z^T\mathbf{W}_{zz}\hat{\mathbf{C}}_z + \mathbf{C}_y^T\mathbf{G}(\hat{\mathbf{G}})^T\mathbf{W}_{uu}\mathbf{G}(\hat{\mathbf{G}})\mathbf{C}_y\right)E\left(\mathbf{x}\mathbf{x}^T\right)\right] \tag{15}$$

so that, defining $\mathbf{\Pi} = E\left(\mathbf{x}\mathbf{x}^T\right)$, we have

$$J = Tr\left(\mathbf{W}_\Lambda\mathbf{\Pi}\right) \tag{16}$$

with $\mathbf{\Pi}$ being the solution of the following Lyapunov equation:

$$\bar{\mathbf{A}}\mathbf{\Pi} + \mathbf{\Pi}\bar{\mathbf{A}}^T + \mathbf{W}_{\mathbf{\Pi}} = 0 \tag{17}$$

where $\mathbf{W}_\Lambda$, $\mathbf{W}_{\mathbf{\Pi}}$, (re)extended to explicitly show $\mathbf{G}(\hat{\mathbf{G}})$, are:

$$\mathbf{W}_{\mathbf{\Lambda}}(\mathbf{G}(\hat{\mathbf{G}})) = \mathbf{Q}_{xx} - \mathbf{Q}_{xu}\mathbf{G}(\hat{\mathbf{G}})\mathbf{C}_y - \mathbf{C}_y^T\mathbf{G}(\hat{\mathbf{G}})^T\mathbf{Q}_{xu}^T + \mathbf{C}_y^T\mathbf{G}(\hat{\mathbf{G}})^T\mathbf{Q}_{uu}\mathbf{G}(\hat{\mathbf{G}})\mathbf{C}_y \tag{18a}$$

$$\mathbf{W}_{\mathbf{\Pi}}(\mathbf{G}(\hat{\mathbf{G}})) = \mathbf{S}_{xx} - \mathbf{S}_{yx}^T\mathbf{G}(\hat{\mathbf{G}})^T\mathbf{B}_u^T - \mathbf{B}_u\mathbf{G}(\hat{\mathbf{G}})\mathbf{S}_{yx} + \mathbf{B}_u\mathbf{G}(\hat{\mathbf{G}})\mathbf{S}_{yy}\mathbf{G}(\hat{\mathbf{G}})^T\mathbf{B}_u^T \tag{18b}$$

with:

$$\mathbf{Q}_{xx} = \mathbf{C}_z^T\mathbf{W}_{zz}\mathbf{C}_z; \qquad \mathbf{Q}_{xu} = \mathbf{C}_{zx}^T\mathbf{W}_{zz}\mathbf{D}_{zu}; \qquad \mathbf{Q}_{uu} = \mathbf{D}_{zu}^T\mathbf{W}_{zz}\mathbf{D}_{zu} + \mathbf{W}_{uu}, \tag{19}$$

and

$$\mathbf{S}_{xx} = \mathbf{B}_d\mathbf{W}_{dd}\mathbf{B}_d^T; \qquad \mathbf{S}_{yx} = \mathbf{D}_{yd}\mathbf{W}_{dd}\mathbf{B}_d^T + \mathbf{W}_{nd}\mathbf{B}_d^T;$$
$$\mathbf{S}_{yy} = \mathbf{D}_{yd}\mathbf{W}_{dd}\mathbf{D}_{yd}^T + \mathbf{W}_{nd}\mathbf{D}_{yd}^T + \mathbf{D}_{yd}\mathbf{W}_{dn} + \mathbf{W}_{nn} \tag{20}$$

Within such a framework the optimization cycle will be based on a numerical optimization, either constrained or unconstrained depending upon the specific design at hand. Therefore, having set the determination of the optimization objective through Eq. 16, considering for the sake of brevity the unconstrained optimization problem of interest in this work and aiming at a full freedom in choosing a performing optimization algorithm, we have to evaluate the objective function, its gradient ad Hessian matrix. In such a view, following a well known approach [27, p. 434] the first derivative of J with respect to a generic design parameter u can be simplified, by avoiding any differentiation of $\mathbf{\Pi}$, though the adjoint Lyapunov equation:

$$\mathbf{\Lambda}\bar{\mathbf{A}} + \bar{\mathbf{A}}^T\mathbf{\Lambda} + \mathbf{W}_{\mathbf{\Lambda}} = 0 \tag{21}$$

so that

$$J_{/u} = Tr\left(\mathbf{W}_{\mathbf{\Lambda}/u}\mathbf{\Pi} + \mathbf{W}_{\mathbf{\Lambda}}\mathbf{\Pi}_{/u}\right) = Tr\left(\mathbf{W}_{\mathbf{\Lambda}/u}\mathbf{\Pi} + 2\mathbf{\Lambda}\bar{\mathbf{A}}_{/u}\mathbf{\Pi} + \mathbf{\Lambda}\mathbf{W}_{\mathbf{\Pi}/u}\right)$$

whose final expression requires just the solution of two Lyapunov equations for the computation of the matrices $\mathbf{\Pi}$ and $\mathbf{\Lambda}$, in place of the n_p needed for computing the $\mathbf{\Pi}_{/u}$ sensitivities associated to the trivial adoption of its left parent form. Nevertheless, to proceed to the calculation of the Hessian matrix $J_{/uv}$, where u and v are generic design parameters, we continue from its left expression, $J_{/u} = Tr\left(\mathbf{W}_{\mathbf{\Lambda}/u}\mathbf{\Pi} + \mathbf{W}_{\mathbf{\Lambda}}\mathbf{\Pi}_{/u}\right)$, so that,

$$J_{/uv} = \frac{1}{2}Tr\left[\mathbf{W}_{\mathbf{\Lambda}/uv}\mathbf{\Pi} + \mathbf{W}_{\mathbf{\Lambda}/u}\mathbf{\Pi}_{/v} + \mathbf{W}_{\mathbf{\Lambda}/v}\mathbf{\Pi}_{/u} + \mathbf{W}_{\mathbf{\Lambda}}\mathbf{\Pi}_{/uv}\right]$$

Then, exploiting matrix commutativity under the trace operator and substituting $\mathbf{W}_{\mathbf{\Lambda}} = -(\mathbf{\Lambda}\bar{\mathbf{A}} + \bar{\mathbf{A}}^T\mathbf{\Lambda})$, from Eq. 21, in the above equation, we are led to:

$$J_{/uv} = \frac{1}{2}Tr\left[\mathbf{W}_{\mathbf{\Lambda}/uv}\mathbf{\Pi} + \mathbf{W}_{\mathbf{\Lambda}/u}\mathbf{\Pi}_{/v} + \mathbf{W}_{\mathbf{\Lambda}/v}\mathbf{\Pi}_{/u} - \mathbf{\Lambda}\left(\bar{\mathbf{A}}\mathbf{\Pi}_{/uv} + \mathbf{\Pi}_{/uv}\bar{\mathbf{A}}^T\right)\right] \tag{22}$$

whose term, $\left(\bar{\mathbf{A}}\mathbf{\Pi}_{/uv} + \mathbf{\Pi}_{/uv}\bar{\mathbf{A}}^T\right)$, containing the second derivatives of $\mathbf{\Pi}$, can be modified so to avoid having them in the Hessian matrix. In fact, taking the second derivative of Eq. 17 we obtain:

$$\bar{\mathbf{A}}\mathbf{\Pi}_{/uv} + \mathbf{\Pi}_{/uv}\bar{\mathbf{A}}^T = \bar{\mathbf{A}}_{/uv}\mathbf{\Pi} + \mathbf{\Pi}\bar{\mathbf{A}}^T_{/uv} + \bar{\mathbf{A}}_{/v}\mathbf{\Pi}_{/u} + \mathbf{\Pi}_{/u}\bar{\mathbf{A}}^T_{/v} + \bar{\mathbf{A}}_{/u}\mathbf{\Pi}_{/v} + \mathbf{\Pi}_{/v}\bar{\mathbf{A}}^T_{/u} + \mathbf{W}_{\mathbf{\Pi}/uv}$$

so that the substitution of its left hand side in Eq. 22, after a few matrix commutations and reassemblies under trace, leads to:

$$\begin{aligned} J_{/uv} = \frac{1}{2}Tr\Big[&\mathbf{W}_{\mathbf{\Lambda}/uv}\mathbf{\Pi} + \mathbf{\Lambda}\mathbf{W}_{\mathbf{\Pi}/uv} + 2\mathbf{\Lambda}\bar{\mathbf{A}}_{/uv}\mathbf{\Pi} + \left(\mathbf{W}_{\mathbf{\Lambda}/u} + \mathbf{\Lambda}\bar{\mathbf{A}}_{/u} + \bar{\mathbf{A}}^T_{/u}\mathbf{\Lambda}\right)\mathbf{\Pi}_{/v} \\ &+ \left(\mathbf{W}_{\mathbf{\Lambda}/v} + \mathbf{\Lambda}\bar{\mathbf{A}}_{/v} + \bar{\mathbf{A}}^T_{/v}\mathbf{\Lambda}\right)\mathbf{\Pi}_{/u}\Big] \end{aligned} \tag{23}$$

thus ending with the need of computing only the first n_p derivatives of $\mathbf{\Pi}$:

$$\bar{\mathbf{A}}\mathbf{\Pi}_{/u} + \mathbf{\Pi}_{/u}\bar{\mathbf{A}}^T + \bar{\mathbf{A}}_{/u}\mathbf{\Pi} + \mathbf{\Pi}\bar{\mathbf{A}}^T_{/u} + \mathbf{W}_{\mathbf{\Pi}/u} = 0 \tag{24}$$

along with the two evaluation of $\mathbf{\Pi}$ and $\mathbf{\Lambda}$, required for the objective function and its gradient. All the $(n_p + 2)$ Lyapunov equations are associated to the same dynamic system, having the closed loop state matrix $\hat{\mathbf{A}}$. At each iteration, it is then possible to apply a similarity transformation setting it into a form more convenient for the effective solution of the $(n_p + 2)$ Lyapunov equations.

Moreover, to avoid the expensive repeated back substitutions of the transformed solutions needed for computing the quadratic performance in term of the untransformed state, such transformations are applied also to the weight and variance matrices, once for all at each iteration. The standard, numerically stable approach, is based on a reduction of $\hat{\mathbf{A}}$ to a Schur form [6], making it possible to solve the transformed equations with a computational cost of the order of $(n_p+2)O(n^3)$ floating point operations. Somewhat more efficient formulations are also viable, e.g. Schur-Hessemberg forms [18, p. 269], but they will remain of the $O(n^3)$ type. A significantly more efficient approach, $(n_p+2)O(n^2)$, is possible by using a transformation based on the closed loop eigenvectors. It is nonetheless often plagued by a significant bad conditioning, making it unsuitable for its repeated blind application in an optimization procedure, often leading to a premature termination of the optimization or to a difficult convergence to the optimum. Thus, while being not to be excluded a priori, it requires a well founded knowledge of the impact of its conditioning on the problem at hand. A solution which allows to choose the best compromise between the Schur and eigenvector transformation, while granting an acceptable numerical conditioning, is the adoption of a block Schur diagonalization [7], [47] [22, p. 397]. In fact, it will provide the most sparse block form of $\hat{\mathbf{A}}$ obtainable for a given acceptable conditioning. Depending on eigenvalues clustering, it will thus lead to a Hessian calculation cost in between $(n_p+2)O(n^3)$ and $(n_p+2)O(n^2)$, at the expense of a factorization cost which, even if it could skyrocket to $O(n^4)$, is mostly only up to fifty per cent, often less, greater than that of a plain Schur form [7], [47]. As discussed in [7] the numerical conditioning of the transformation matrix can become very bad if clustered eigenvalues belonging to marginally separated eigenspaces are forced into different blocks. Therefore, the eigenstructure of the state matrix is the main factor driving the size of the diagonal blocks of the resulting Schur matrix. It should be remarked that the determination of a numerically acceptable block diagonal structure embedded in the determination of a block diagonal Schur form needs not to be carried out at each iteration. In fact, since the block structure tends to stabilize as the optimization progresses, it can be assigned a priori to the Schur factorizing function, thus avoiding the block reordering part of the algorithm, with a reduction of the related computational time.

B. Optimization algorithm

Despite the availability of many effective optimization codes, it has been verified that it is possible to reach a faster solution with the implementation of the Levenberg-Marquardt algorithm [25], [37, p. 262] and [26, p. 47], here described.

Given our objective function $J(\mathbf{g})$, $\mathbf{g} \in \mathbb{R}^n$, $\mathbf{g}$ being the vectorization of $\hat{\mathbf{G}}$, with gradient $\mathbf{f}(\mathbf{g}) \in \mathbb{R}^n$ and Hessian $\mathbf{H}(\mathbf{g}) \in \mathbb{R}^{n \times n}$, the algorithm provides the iteration $\mathbf{g}^{k+1} = \mathbf{g}^k + \Delta\mathbf{g}$ by solving a sequence of unconstrained quadratic approximations of the form

$$\min_{\Delta\mathbf{g} \in \mathbb{R}^n} \tilde{J}(\Delta\mathbf{g}) = \min_{\Delta\mathbf{g} \in \mathbb{R}^n} \left[J(\mathbf{g}^k) + \mathbf{f}(\mathbf{g}^k)^T \Delta\mathbf{g} + \frac{1}{2} \Delta\mathbf{g}^T \left(\mathbf{H}(\mathbf{g}^k) + \lambda^2 Diag[\mathbf{H}(\mathbf{g}^k)] \right) \Delta\mathbf{g} \right] \tag{25}$$

where $\mathbf{g}^k$ is the solution available from the previous step and $\Delta\mathbf{g}$ its increment toward $\mathbf{g}^{k+1}$, λ^2 being introduced to assure a reduction of $J(\mathbf{g})$ while limiting the magnitude of $\Delta\mathbf{g}$. Since the cost function and its derivatives are defined only for a stable system, a necessary condition for the convergence of the procedure, the safeguarding of such a property throughout the whole optimization is a must. Therefore, as the objective function will grow when approaching the stability boundary, the step magnitude containment will automatically maintain the solution search within the set of stabilizing solutions. Thus, there remains only the need of initiating the algorithm with an asymptotically stable closed loop system. Consequently, whenever the system at hand is not so already, the non trivial problem of providing an appropriate initial SOF $\hat{\mathbf{G}}$ has to be solved. Possible solutions can be devised by adopting the penalty shift method described in [33] or an initial full state controller whose contribution is driven to the constrained SOF structure through a continued optimization procedure.

The above Levenberg-Marquardt scheme can be seen as a modified Newton-Raphson solution of the stationary condition $\mathbf{f}(\mathbf{g}^k) = 0$, i.e.

$$\left[\mathbf{H}(\mathbf{g}^k) + \lambda^2 Diag[\mathbf{H}(\mathbf{g}^k)] \right] \Delta\mathbf{g} + \mathbf{f}(\mathbf{g}^k) = 0 \tag{26}$$

In such a view, when its zero is approached, as witnessed both by a small step length $\Delta\mathbf{g}^k$ and factor λ, significant improvements can be provided by a plain modified Newton-Raphson iteration, i.e. keeping $\mathbf{H}(\mathbf{g}^k)$ constant, possibly improved, almost for free, through BFGS updates [25, p. 113], [37, p. 198] and [26, p. 71]. By limiting the number of Hessian evaluations the latter variation can

further enhance the computational efficiency of our Hessian based approximation.

C. Comparing Computational Performancees

After remarking that the above optimization scheme has shown better or equal results over alternative methods reported in the literature [39] [30] [45], for a set of simple and commonly used examples. An overview of the performances related to its application in this paper is now shown, it is based on a sample of the design results to be presented next and is related to the most computationally demanding configuration with 153 states, three control surfaces and a fully coupled SOF (3 output $\times$ 34 measures = 102 elements) gain matrix. The related block diagonal Schur form has a single, relatively large, block of 36 elements, associated to the double integrators, all the rest being of 1 or 2 terms. Before the optimization all variables were scaled, using the related maximum values obtained through an open loop simulation. The presented results, as well as the following design procedure, have been obtained by using a single core of a four cores personal computer, with an INTEL i7-3630QM processor, a clock frequency of 2.4 GHz and 6 Gb RAM. The optimization was assumed to have converged when both a tolerance of 10^{-4} on the relative gain changes and of 10^{-5} on the relative change of the objective function were satisfied, using the gradient as a further a posteriori convergence verification. The outcomes of different optimization algorithms are summarized in Tab. (3), where the initial solution had $J = 106.73$.

order	Algorithm	Lyapunov solution	Number of Evaluations			Cost Function	Norm of gradient	Time [s]
			J	$\mathbf{f}$	$\mathbf{H}$			
first	BFGS	Schur	555	555	–	85.1883	1.71×10^{-3}	11.14
first	BFGS	BdSchur	554	554	–	85.1883	1.71×10^{-3}	12.11
second	LM	Schur	56	17	17	85.1837	6.54×10^{-6}	8.45
second	LM	BdSchur	47	14	14	85.1837	1.45×10^{-6}	5.42
second	LM-BFGS	Schur	50	17	12	85.1837	5.30×10^{-5}	6.16
second	LM-BFGS	BdSchur	44	16	11	85.1837	4.39×10^{-5}	4.38

Table 3 *Results obtained by using different optimization algorithms.*

It should be noticed that the, supposedly state of the art, Quasi-Newton-BFGS method, as implemented in Matlab function `fminunc`, was used for the first-order, gradient only, based optimization. Then, after remarking that the core cost, associated to computing any of the two used

Schur forms and the solution of the Lyapunov equations, is the same for all the shown results, the above table makes it clear that the Hessian based approach clearly benefits from using the block diagonal form, while the gradient based results do not, albeit only marginally. Moreover, at least for the size of the problem under scrutiny, it is evident that the number of Lyapunov solutions is much higher for the Hessian based, (11 to 17)$\times$102, than for the gradient based solutions, (554 to 555)$\times$2. The above remarks clearly addresses the fact that, once a Schur form is available, a Lyapunov solutions costs significantly less than a Schur factorization. A fact witnessed by the sizeable time gain of the Hessian base methods, all showing a roughly close number of optimization cycles, i.e. for almost the same number of Schur factorizations. In fact it has been verified that a block diagonalized Lyapunov solution is approximately half of that related to a full Schur form. A further evidence of the above statement comes from the gradient based approach for which, having to solve just two Lyapunov equations for each iteration, the adoption of the block diagonal form causes an increased computational time, roughly 10%, in accordance with the measured time differences between the two different Schur factorization. It is then to be remarked that, for the application at hand, such a cost is well below the practical 50% upper bound suggested in [7], [47]. Such a point evidences furthermore that much of the computational cost per iteration is associated to the Schur factorization.

Along with the above highlighted points it appears that the gradient based optimizations failed to reach a precise stationary point, ending with an $O(10^{-3})$ gradient norm, despite its high number of optimization cycles, 555. Such a somewhat incomplete, albeit acceptable, convergence is likely due to the fact that J is fairly flat near the minimum and the quasi-Newton method misses the aim of reconstructing a Hessian matrix adequate enough to achieve the required step increments. It is thus clear that the Hessian based approach leads to a significant reduction of the computational time required for a well converged optimization. Within its framework, the advantage of adopting a block diagonal Schur form is always significant, perhaps with the unexpected effect that a reduction of its conditioning, produces a small reduction of the number of iterations to convergence. Moreover, the modified Newton-Raphson method, with BFGS updates, further reduces the computational cost of the Hessian based optimization, making it a premium choice for the design of our SOF based load

alleviator.

As said, all the presented results have been obtained with a single CPU. So, it is worth pointing out that the Hessian based method can linearly scale its performances through a trivial large grain parallelization of its, numerous but independently solvable, Lyapunov equations. A scaling that will be limited only to a factor of two for a gradient only based optimization.

As the design of a control system may require many iterations to appropriately tune the cost function capable of providing a controller meeting all the design specifications, it is clearly of the utmost importance to exploit the fastest possible optimizer.

V. Final Design and Verifications

The here preferred SOF controller will be compared against a reference solution based on a standard LQG-LTR design [19]. The adopted LTR procedure provides a full order observer based controller with a $\pm 11.1\ dB$ gain and $\pm 62.3^{\circ}$ phase margins at its input. However, to be closer to a real implementation its validation is based on a reduced order realization. Then, using a Hankel norm based reduction of its transfer function [43], it is possible to maintain a gain margin of $\pm 7.46\ dB$ and a phase margin of $\pm 44.10^{\circ}$ with just 56 states, out of the original 153.

The leading parameter driving the quadratic design objective is the ratio between the control weights $\mathbf{W}_{zz}$ and $\mathbf{W}_{uu}$, which is chosen to achieve an appropriate trade off between the optimization of the leading performance, i.e. the wing root bendingi moment, and the need to contain the activity of the control surfaces.

Moreover, in order to avoid the subtraction of an excessive elevator excursion to a possible external flight control system, its authority was somewhat reduced with respect to that allowed to the ailerons, by increasing its weight $\mathbf{W}_{uu}$.

It should be remarked that, both for the LQG-LTR and SOF controller, the performances of the adopted quadratic index are, either explicitly or implicitly, of the frequency weighted kind. In fact so are the objective responses, containing only components within the state bandwidth, while the aileron rotation, which is the actual control force generator, is frequency weighted the opposite way through its transfer function.

A. Reference Design Model and Validation

Despite a model of not so trivial size, the numerical efficiency of the previously illustrated controller optimization allows to viably tackle weighted multi model designs. Nevertheless both a few tries of such an approach and extensive simulations suggested that, with enough confidence, a single design based on a well chosen discrete gust at a well chosen flight condition would provide a solution capable of a load alleviation over a range of different flight conditions. The determined reference design is at $h = 8000\ m$, $M_\infty = 0.71$, $q_\infty = 12.826 \times 10^3\ Pa$, for a worst discrete *1-cos* gust providing the highest peak wing root bending moment with $H = 40\ m$.

After the design all simulated validations will add the sensor disturbances given in the following list:

- accelerometers: offset of plus uniform white noise with amplitude 5% of the measurement range;
- acceleration integrators: offset of plus uniform white noise, both with amplitude 1% of the measurement range;
- velocity integrators: offset plus uniform white noise, both with amplitude 1% of the measurement range;
- IMU: uniform white noise with amplitude 5% of the measurement range;

It should be remarked that the offset disturbances for the high pass integrated sensing units is more a kind of checking of the simulation code than something of real value.

Possible actuator saturations were accounted for with:

- control surface deflections: $\pm 10°$, authority allowed to the load alleviation, the overall value doubled;
- control surface deflection rates: $\pm 50\ deg/s$;
- stall hinge moment: the steady state hinge moment at full overall deflection.

All the related simulations were carried out using the explicit, second order, Heun method, with

a time step of 5×10^{-4} s, adequate for caring of any saturation-desaturation instant just at the end of each time step.

B. Validation and Chosen Final Design

The first part of the validations was aimed at checking the pros and cons of a segmented aileron with respect to a unified deflection of the its two parts. For such cases no constraint was imposed to the structure of the gain matrix $\hat{\mathbf{G}}$ and thus all the wing and tail measurements were fed back to both the aileron and the elevator. To obtain a fair comparison between the two configurations, the related weighting matrices were selected in a way providing gain and phase margins closed to: ± 7.50 dB and $\pm 45°$.

The wing root bending moment obtained in the two cases is displayed in Fig. 6a, showing that the split aileron is capable of a slightly better bending moment reduction. Fig. 6b, shows that such a reduction is obtained through an incremented deflection of the inboard aileron, while the outboard aileron has a lower deflection, both being adequately contained and far away from any saturation.

Having chosen the split aileron solution, the effect of imposing a partially decentralized structure on $\hat{\mathbf{G}}$ has then been tested, once more adjusting the design cost function of the new solution so to maintain margins close to those of the single aileron. The split controller has now only 76 free gains, against 102 of the its full counterpart, a gain margin of ± 7.14 dB and a phase margin of $\pm 42.53°$, see Fig. (7), eventually making it the preferred solution. Fig. 7 shows also he response of the dynamic LQG-LTR controller. As it can be seen the SOF performances are comparable with those of the more complex LQG-LTR controller, the wing root bending moment peak being reduced by a 23.5% with the former, against a marginally better 26% of the latter, mostly related to the fact that it can exploit its explicit knowledge of the discrete gust through the observer.

From Fig. 8, it is possible to ascertain that the deflection of the control surfaces is always well below their allowed saturations, the inboard aileron having a larger motion, up to a peak value of $5.9°$. A saturation of the deflection rate is reached by the inboard aileron, as shown in Fig. 9. The fact that the controller fulfills is task even when such a saturation appears for a relatively sizeable time lapse is an indications of the possible robustness of the SOF design.

It should be also remarked that the bending moment alleviation is obtained through an in-

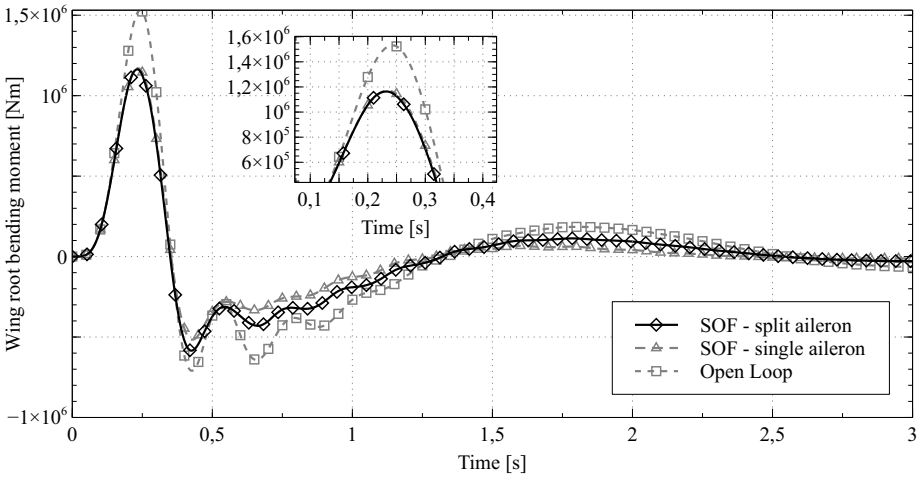

(a) *Wing root bending moment.*

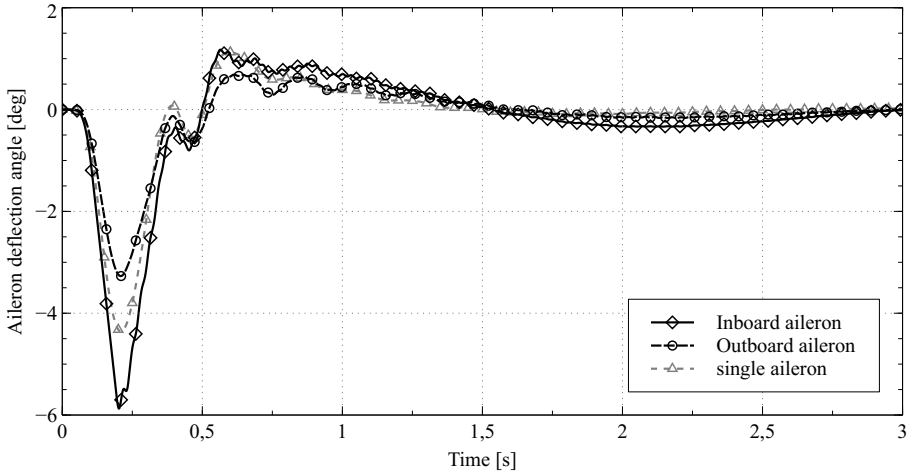

(b) *Control surface deflections.*

Fig. 6 *Single and split aileron performances,* $H = 40\ m$. $h = 8000\ m$, $M = 0.71$, $q_\infty = 12.826 \times 10^3\ Pa$.

creased peak of the torsional moment, as shown in Fig 10. Nonetheless, the controller is capable of attenuating the torsional moment along the rest of the response, as further witnessed by the Power Spectral Density (PSD) plots of Figs. 11a and 11b. They show a comprehensive overall effectiveness in limiting continuous turbulence loads, both in bending and torsion, confirming also what suggested by the initial design familiarization phase. It is furthermore noticed that such a figure contains an indication of the possible improvements obtainable with an increased elevator bandwidth, up to the same as that of the ailerons. To provide a more complete picture of the effectiveness of the

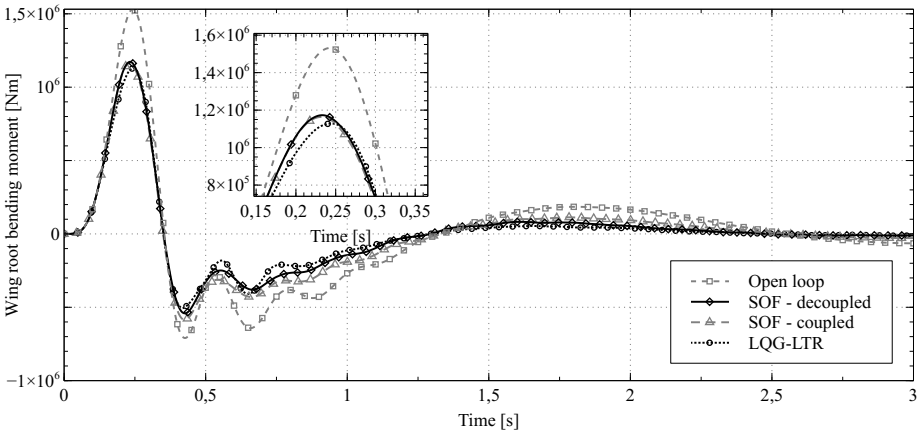

Fig. 7 *Full and decoupled controller performances,* $H = 40\ m.\ h = 8000\ m,\ M = 0.71,$ $q_\infty = 12.826 \times 10^3\ Pa.$

partially decentralized controller, Fig. (12) displays the PSD of the vertical accelerations, related to ride qualities weighted within the performance index.

The improved peak bending moments for discrete gusts having gradients over the range between 18 and 110 meters are shown in Fig. 14. Such outcomes should point out that a leading discrete design gust of 40 m was appropriately chosen.

Nevertheless, the response to the shortest gust, i.e. with a gradient of $H = 9\ m$, shown in Fig. 13, displays the somewhat worsened performances related to its higher frequency content. In fact, as shown in Fig. 13b, it demands significantly higher deflection rates, leading to longer saturations. However, Figure Fig. 13a shows that the maximum wing root bending moment is nonetheless reduced, with the static controller giving better performances than the LQG-LTR one. In fact, having embedded the knowledge of the reference discrete gust and flight condition in its design, the latter is strongly biased toward the nominal design, so being significantly affected by discrete gust changes. On the contrary, as it will be shortly shown in the next paragraph, a SOF controller is much more insensitive to changes of the operating conditions.

C. Gain Scheduled Implementation

The reference SOF controller proved to be able to alleviate gust and turbulence loads over the all flight envelope, without destabilizing the system but at the expense of a loss of its margins, from 7.01 dB to 3.59 dB and from 42.34°. Even if such a result indicates that the adopted design frame-

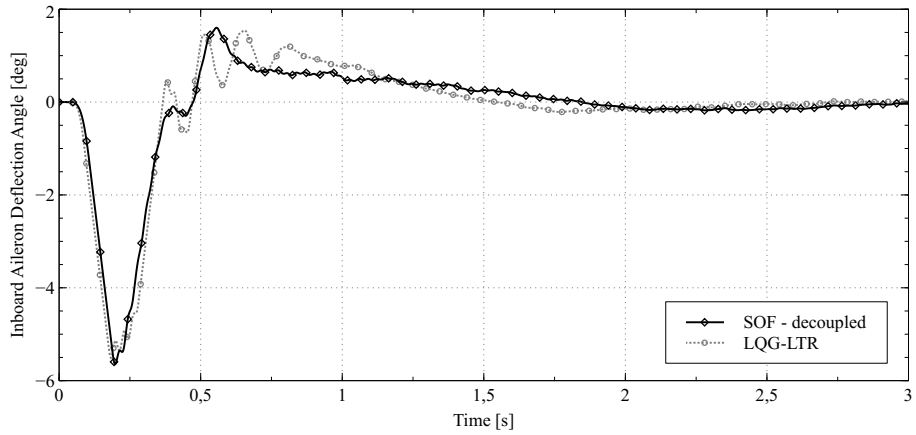

(a) *Inboard aileron.*

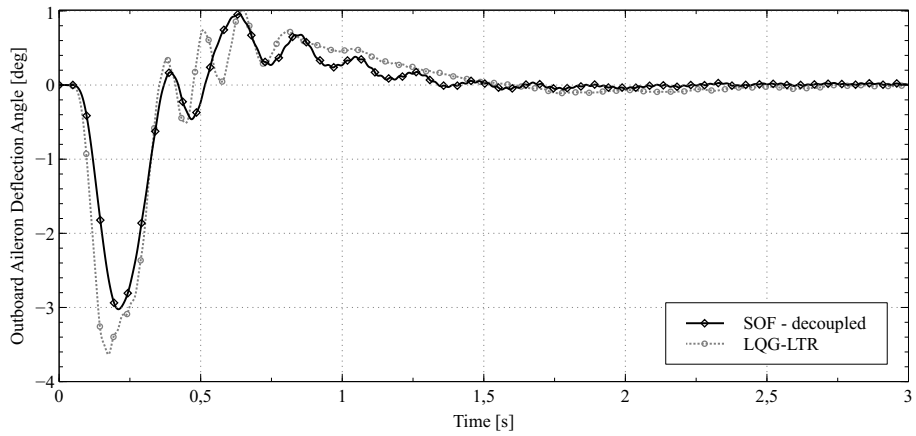

(b) *Outboard aileron.*

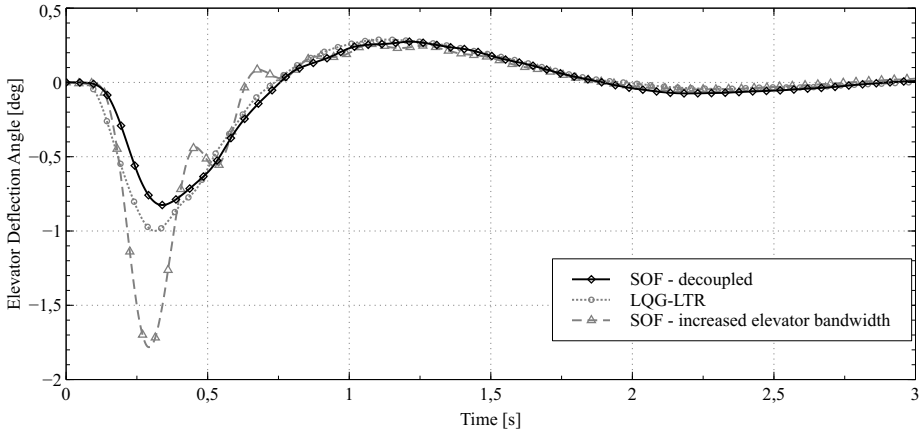

(c) *Elevator.*

Fig. 8 *Control surface deflection,* $H = 40\ m$, $h = 8000\ m$, $M = 0.71$, $q_\infty = 12.826 \times 10^3\ Pa$.

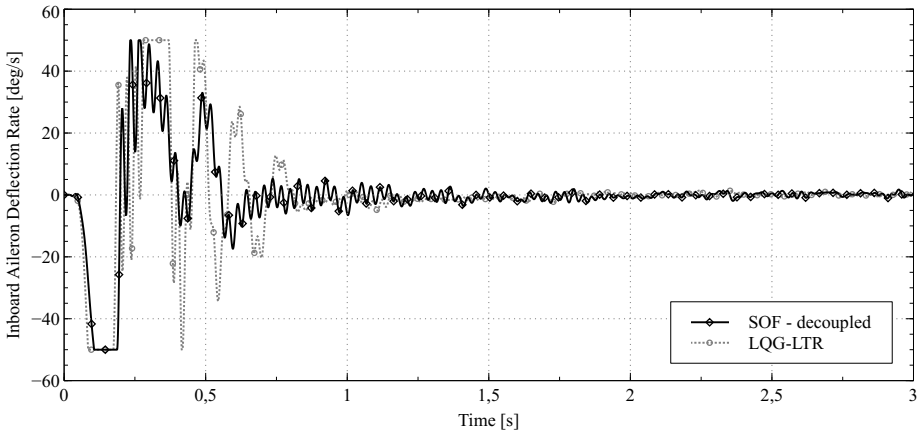

Fig. 9 *Inboard aileron deflection rate,* $H = 40\ m$, $h = 8000\ m$, $M = 0.71$, $q_\infty = 12.826 \times 10^3\ Pa$.

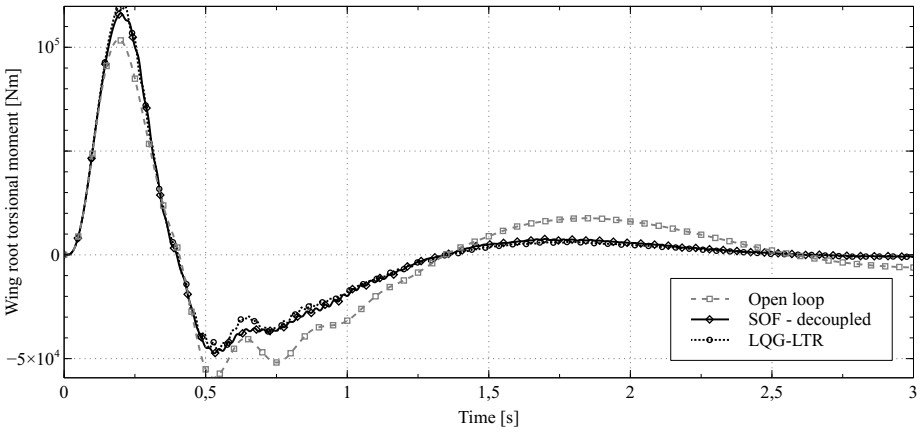

Fig. 10 *Wing root torsional moment,* $H = 40\ m$, $h = 8000\ m$, $M = 0.71$, $q_\infty = 12.826 \times 10^3\ Pa$.

work provides a significant overall robustness, to achieve the best load reduction while maintaining robust margins over the all flight envelope, a gain scheduling is adopted. The algebraic nature of the SOF controller makes it very suitable for a trivial scheduling, based on pure per gain element bilinear algebraic interpolation, over a set of gain matrices designed at a discrete set of operational conditions.

The reference designs are then carried out over the following assigned values of the flight envelope: M_∞: 0.5, 0.6, 0.71, 0.8; $q_\infty(Pa)$: 5.9625×10^3, 12.826×10^3 and 20.776×10^3.

In order to keep adequately safe margins and acceptable performances, the weights used in the definition of the cost function were appropriately set for each design point. In fact, because of the high torsional stiffness, higher dynamic pressures increase the aerodynamic forces and the

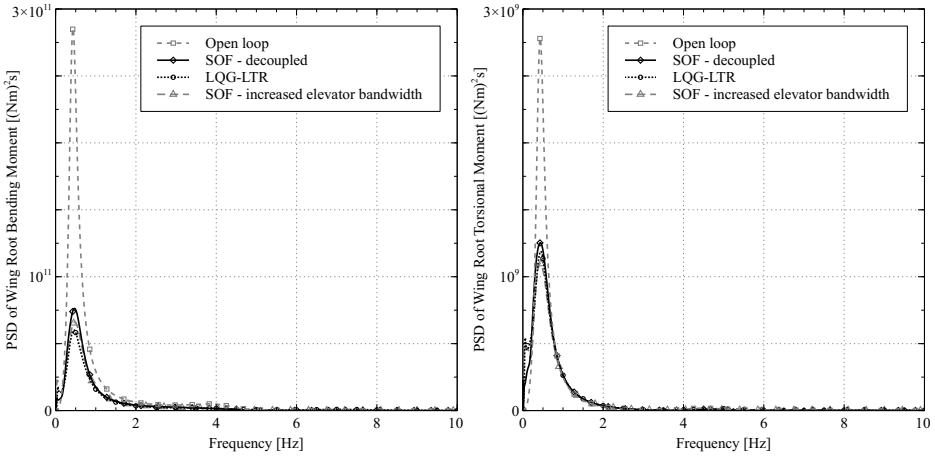

(a) *Bending moment.* **(b)** *Torsional moment.*

Fig. 11 *Wing root bending and torsional moment PSDs,* $L = 300\ m$, $h = 8000\ m$, $M = 0.71$, $q_\infty = 12.826 \times 10^3\ Pa$.

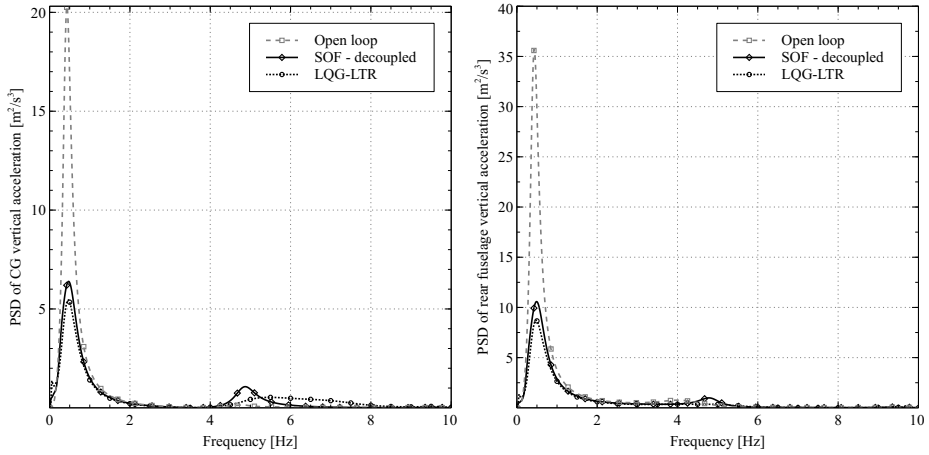

(a) *Centre of gravity.* **(b)** *Tail root.*

Fig. 12 *Vertical acceleration PSDs,* $L = 300\ m$, $h = 8000\ m$, $M = 0.71$, $q_\infty = 12.826 \times 10^3\ Pa$.

control activity must be reduced to maintain an acceptable robustness. On the contrary, the control activity can be increased at lower dynamic pressures, without affecting the robustness properties of the controllers. It should be pointed out that, to speed up the repeated designs of the gain matrices, it is possible to use as initial guess the controller optimized at its closer design point. Since there are not dramatic variations of the system and its cost function, such a rough continuation procedure greatly reduces the number of iterations with respect to a cold start, typically by a factor two at

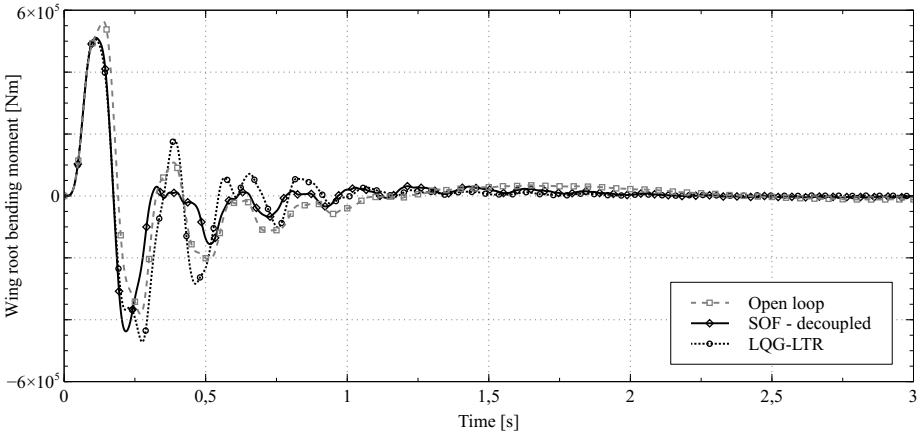

(a) *Wing root bending moment.*

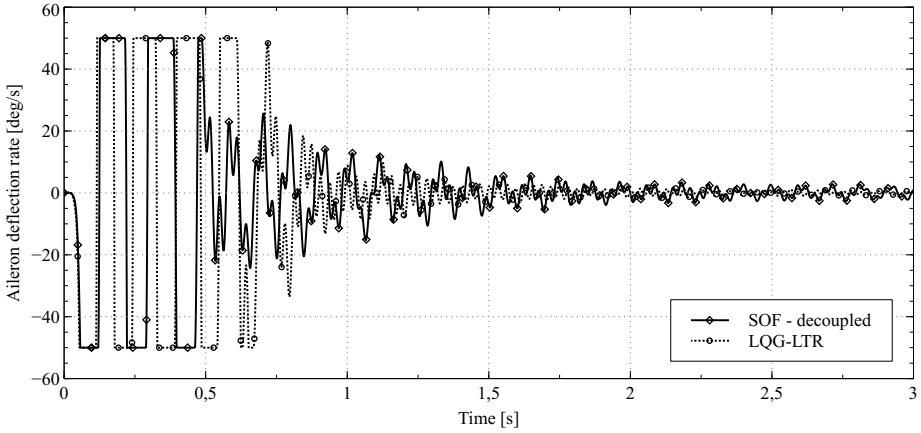

(b) *Inboard aileron deflection rate.*

Fig. 13 *Short gust response,* $H = 9\ m$, $h = 8000\ m$, $M = 0.71$, $q_\infty = 12.826 \times 10^3\ Pa$.

least.

Figure Fig. 15 shows the peak wing root bending moments and the inboard aileron deflections at a set of differing flight conditions with a gust gradient of $H = 40\ m$. It is recalled that the reference controller was designed for Mach $M = 0.71$ and $q_\infty = 12.826 \times 10^3\ Pa$, It can be seen that at higher speeds the reference controller is even more effective than the properly scheduled local one, albeit at the expense of already mentioned margin reductions. On the contrary the local controller has more authority at lower speeds, and thus is more effective. The maximum aileron deflection, shown in Fig. 15b, is a further indication of the greater activity of the local controller at lower speeds which is instead lowered at higher speeds.

Figure Fig. 16 shows the variance of the response to a continuous turbulent excitation. The same

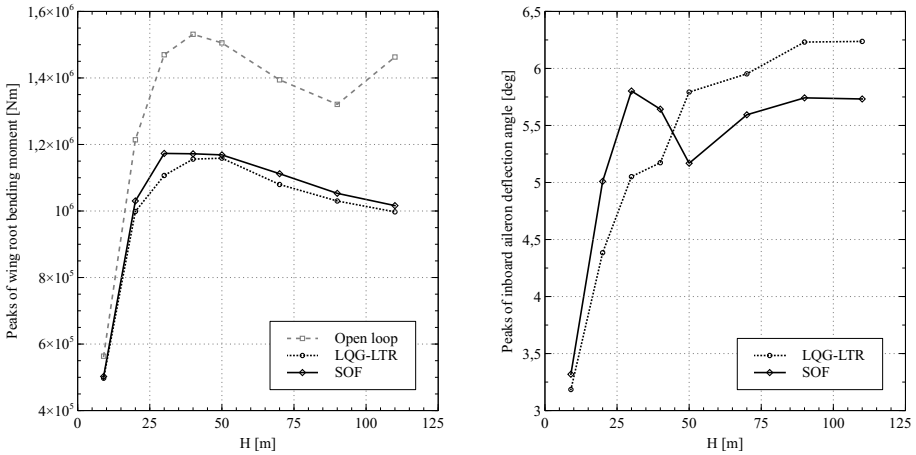

(a) *Wing root bending moment.* **(b)** *Inboard aileron deflection angle.*

Fig. 14 *Samples of peak responses for different gust gradients,* $h = 8000\ m$, $M = 0.71$, $q_\infty = 12.826 \times 10^3\ Pa$.

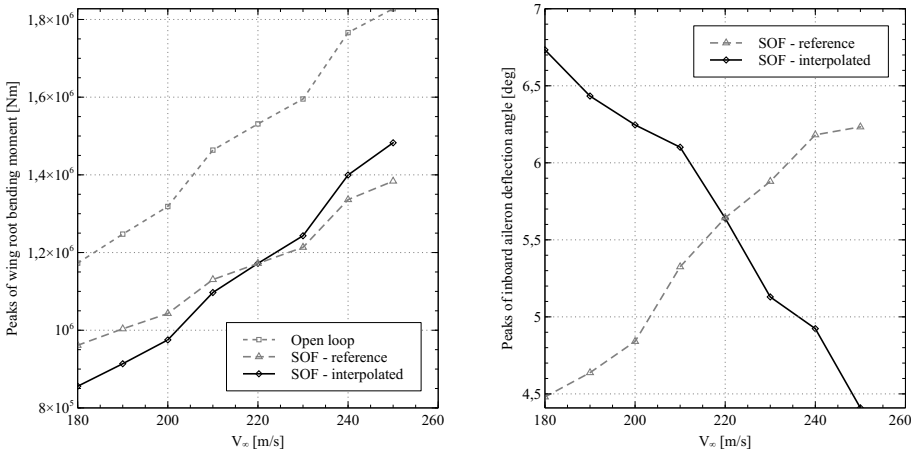

(a) *Wing root bending moment.* **(b)** *Inboard aileron deflection angle.*

Fig. 15 *Samples of peak responses at different flight conditions* $H = 40\ m$.

behaviour found for the peak responses is confirmed, showing, once more, that the deterministic design provides a controller capable of alleviating both the deterministic and the stochastic loads.

VI. Conclusions

The SOF design of an active gust/turbulence load alleviation presented in this paper provides a simple, partially decentralized, controller whose performances are comparable to those of a robustified LQG-LTR design. The simple and straightforward second order, Hessian based, optimization

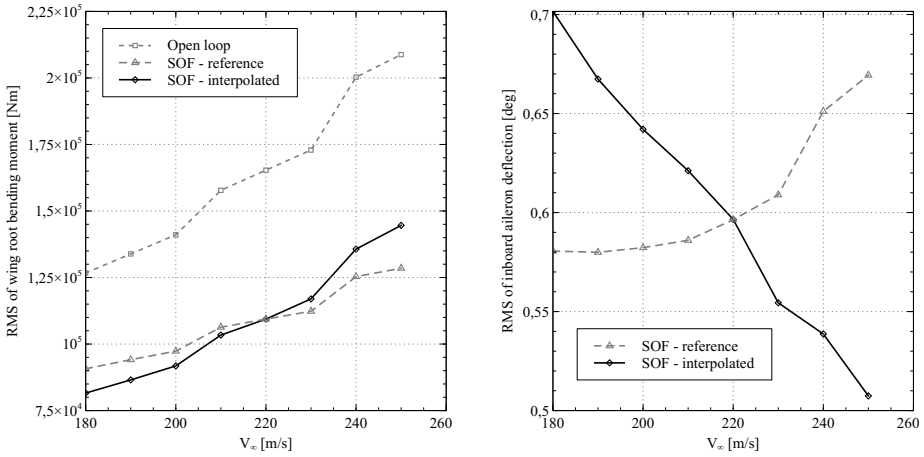

(a) *Wing root bending moment.* **(b)** *Inboard aileron deflection angle.*

Fig. 16 *Sample response variances at different flight conditions* $H = 40\ m$.

procedure adopted for its design, combined with block diagonal Schur factorizations, shows significant computational improvements with respect to state of the art gradient based Quasi-Newton methods. The effective SOF controller has been designed with reference to a well chosen worst discrete gust and reference flight condition, resulting in a good solution also for a continuous turbulence. Beside the quite acceptable gain and phase margins it can achieve, its robustness is further proven by its capability to remain effective over a significantly, wider set, of flight conditions. Yet, to regain adequate margins over the whole flight envelope, a scheduled solution is eventually adopted, whereas the algebraic nature of the SOF controller makes it possible a scheduling based on a simple bilinear algebraic interpolation over just a few reference designs.

References

[1] AAVV. Certification Specifications for Large Aeroplanes CS-25. amendment 7 ed., European Aviation Safety Agency, October 2009. Annex to ED Decision 2009/013/R.

[2] E. Albano and W. P. Rodden. A Doublet-Lattice Method for Calculating Lift Distribution on Oscillating Surfaces in Subsonic Flow. *AIAA Journal*, 7(2):279–285, 1969.

[3] B D O Anderson and J B Moore. *Linear Optimal Control*. Englewood Cliffs, NJ, 1971.

[4] J. I. Arnold and J. B. Dempster. Flight Test Evaluation of an Advanced Stability Augmentation System for B-52 Aircraft. *Journal of Aircraft*, 6(4):343–348, 1969.

[5] Alessandro Astolfi and Patrizio Colaneri. A Hamilton–Jacobi Setup for the Static Output Feedback Stabilization of Nonlinear Systems. *Automatic Control, IEEE Transactions on*, 47(12):2038–2041, 2002.

[6] R.H. Bartels and G.W. Stewart. Algorithm 432: Solution of the Matrix Equation AX + XB = C. *Comm. ACM*, 15:820–826, 1972.

[7] C. A. Bavely and G.W. Stewart. An Algorithm for Computing Reducing Subspaces by Block Diagonalization. *SIAM Journal on Numerical Analysis*, 16(2):359–367, 1979. doi:10.1137/0716028.

[8] S. Bingulac, N Cuk, and M Calovic. Calculation of optimum feedback gains for output-constrained regulators. *Automatic Control, IEEE Transactions on*, 20(1):164–166, 1975.

[9] J D Blight, R L Dailey, and D Gangsaas. Practical control law design for aircraft using multivariable techniques. *International Journal of Control*, 59(1):93–137, 1994. doi:10.1080/00207179408923071.

[10] Boeing Commercial Airplane Company. Integrated Application of Active Control (IAAC) Technology to an Advanced Subsonic Transport Project — Initial Act Configuration Design Study. Technical report, NASA, CR–159249, 1980.

[11] S.P. Boyd, L. El Ghaoui, E. Feron, and V. Balakrishnan. *Linear Matrix Inequalities in System and Control Theory*. Siam Studies in Applied Mathematics, 1994. doi:10.1137/1.9781611970777.

[12] R. T. Britt, J. A. Volk, D. R. Dreim, and K. A. Applewhite. Aeroservoelastic Characteristics of the B-2 Bomber and Implications for Future Large Aircraft. Technical report, DTIC Document, 2000.

[13] J R Broussard and N Halyo. Active Flutter Control using Discrete Optimal Constrained Dynamic Compensators. In *American Control Conference, 1983*, pages 1026–1034, 1983.

[14] L. Cavagna, S. Ricci, and L. Riccobene. Structural Sizing, Aeroelastic Analysis, and Optimization in Aircraft Conceptual Design. *Journal of Aircraft*, 48(6):1840–1855, 2011. doi:10.2514/6.2005-1959.

[15] L. Cavagna, S. Ricci, and L. Travaglini. NeoCASS: An integrated Tool for Structural Sizing, Aeroelastic Analysis and MDO at Conceptual Design Level. *Progress in Aerospace Sciences*, 47:621–635, 2011. doi: http://dx.doi.org/10.1016/j.paerosci.2011.08.006.

[16] E. G. Collins, W. M. Haddad, and S. S. Ying. Reduced–Order Dynamic Compensation Using the Hyland–Bernstein Optimal Projection Equations. In *Proceedings of the American Control Conference Seattle, Washington*, June 1995. doi:10.2514/3.21633.

[17] Morteza Dardel and Firooz Bakhtiari-Nejad. Limit cycle oscillation control of wing with static output feedback control method. *Aerospace Science and Technology*, 24(1):147–160, 2013. doi: 10.1016/j.ast.2011.08.013.

[18] Biswa Nath Datta. *Numerical methods for Linear Control Systems*. Elsevier Academic Press: San Diego, CA, U.S.A., London, U.K., 2004.

[19] John Doyle and Guter Stein. Robustness with Observers. *Automatic Control, IEEE Transactions on*, 24(4):607–611, 1979. doi:10.1109/CDC.1978.267883.

[20] Bernard Etkin. Turbulent Wind and Its Effect on Flight. *Journal of Aircraft*, 18(5):327–345, 1981. doi:10.2514/3.57498.

[21] Federico Fonte. Active gust glleviation for a regional aircraft through static output feedback. Master's thesis, Politecnico di Milano, 2013.

[22] Gene H. Golub and Charles F. Van Loan. *Matrix Computations*. The Johns Hopkins University Press, Baltimore, fourth edition, 2013.

[23] K. U. Hahn and R. König. ATTAS Flight Test and Simulation Results of the Advanced Gust Management System LARS. In *AIAA Conf. on Atmosph. Flight Mech., Hilton Head, South Carolina*, 1992. doi:10.2514/6.1992-4343.

[24] S.M. Hoppe. *Gust Alleviation Using Direct Gust Measurement*. National Aeronautics and Space Administration, 2000. URL `http://books.google.it/books?id=OHMoMgAACAAJ`.

[25] Carl T Kelley. *Iterative Methods for Linear and Nonlinear Equations*. SIAM Philadelphia, 1995.

[26] Carl T Kelley. *Iterative Methods for Optimization*. SIAM Philadelphia, 1999.

[27] H. Kwakernaak and R. Sivan. *Linear Optimal Control Systems*. Wiley Interscience, New York, 1972.

[28] William Levine and Michael Athans. On the Determination of the Optimal Constant Output Feedback Gains for Linear Multivariable Systems. *Automatic Control, IEEE Transactions on*, 15(1):44–48, 1970. doi:10.1109/TAC.1970.1099363.

[29] W. P. Lock, E. E. Kordes, J. M. McKay, and Wykes. Flight Investigation of a Structural Mode Control System for the XB-70 Aircraft. Technical report, NASA TN D-7420, 1973.

[30] Yannick Losser. *Ajustement de lois de commande application en aéronautique*. PhD thesis, Ecole nationale supérieure de l'aéronautique et de l'espace, Toulouse, 2006.

[31] D. J. Lucia. The Sensorcraft Configurations: A Non-linear Aeroservoelastic Challenge for Aviation. In *AIAA 2005-1943, 46th AIAA/ASME/ASCE/AHS/ASC Structures, Structural Dynamics & Materials Conference*, 2005. doi:10.2514/6.2005-1943.

[32] Mauro Manetti, Marco Morandini, and Paolo Mantegazza. Completely, partially centralized and fully decentralized control schemes of large adaptive mirrors. *Journal of Vibration and Control*, to appear. ISSN 1077-5463.

[33] P Mantegazza. A Technique to Design Structurally Constrained Stabilizing Control Systems for Actively Controlled Aircraft. *L'Aerotecnica - Missili e Spazio*, 63(3/4):315–317, 1984.

[34] D McLean. Gust-alleviation control systems for aircraft. In *Proceedings of the Institution of Electrical Engineers*, volume 125, pages 675–685, 1978. doi:10.1049/piee.1978.0159.

[35] Y. Miyazawa and E. Dowell. Robust control system design with multiple model approach and its application to active flutter control. In *AIAA 1989-3578, Guidance, Navigation and Control Conference*, 1989. doi:10.2514/6.1989-3578.

[36] D. D. Moerder and A. Calise. Convergence of a numerical algorithm for calculating optimal output feedback gains. *Automatic Control, IEEE Transactions on*, 30(9):900–903, 1985. doi: 10.1109/TAC.1985.1104073.

[37] Jorge Nocedal and Stephen J Wright. *Numerical Optimization*. Springer–Verlag New York, 1999.

[38] Mayuresh J. Patil and Dewey H. Hodges. Output Feedback Control of the Nonlinear Aeroelastic Response of a Slender Wing. *Journal of Guidance, Control, and Dynamics*, 25(2):302–308, 2002. doi: 10.2514/2.4882.

[39] T. Rautert and E. Sachs. Computational Design of Optimal Output Feedback Controllers. *SIAM Journal on Optimization*, 7(3):837–852, 1997. doi:10.1137/S1052623495290441.

[40] C. D. Regan and C. V. Jutte. Survey of Applications of Active Control Technology for Gust Alleviation and New Challenges for Lighter-weight Aircraft. Technical report, NASA, TM–2012-216008, 2012.

[41] M Ripepi and P Mantegazza. Improved Matrix Fraction Approximation of Aerodynamic Transfer Matrices. *AIAA Journal*, 51(5):1156–1173, 2013. doi:10.2514/1.J052009.

[42] W. P. Rodden and E. H. Johnson. *MSC/NASTRAN Aeroelastic Analysis User's Guide*. The MacNeal-Schwendler Corp., Los Angeles, 1994.

[43] M G Safonov, R Y Chiang, and D J N Limebeer. Optimal hankel model reduction for nonminimal systems. *Automatic Control, IEEE Transactions on*, 35(4):496–502, 1990. doi:10.1109/9.52314.

[44] V. L. Syrmos, C. T. Abdallah, P. Dorato, and K. Grigoriadis. Static Output Feedback — A Survey. *Automatica*, 33(2):125–137, 1997. doi:10.1016/S0005-1098(96)00141-0.

[45] H. T. Toivonen and P. M. Mäkilä. Newton's method for solving parametric linear quadratic control problems. *International Journal of Control*, 46(3):897–911, 1987. doi:10.1080/00207178708547402.

[46] M Vajta. Some remarks on padé-approximations. In *Proc. 3rd TEMPUS-INTCOM Symp. Intelligent Systems in Control and Measurement*, pages 53–58, 2000.

[47] A Varga. Computational techniques based on the block-diagonal form for solving large systems modeling problems. In *Proc. IEEE 1993, Conference on Aerospace Control Systems, Westlake Village, CA*, pages 693–697, 1993. doi:10.1109/AEROCS.1993.721023.

[48] J C Yeager. Implementation and Testing of Turbulence Models for the F18-HARV Simulation. *Lockheed Martin Engineering & Sciences, NASA CR-1998-206937*, 1998.

[49] J. W. Youngblood, T. A. Talay, and R. J. Pegg. Design of Long-Endurance Unmanned Airplanes Incorporating Solar and Fuel Cell Propulsion. In *AIAA/SAE/ASME 20th Joint Propulsion Conference, Cincinnati OH*, 1984. doi:10.2514/6.1984-1430.